1-2-2017

Three-Dimensional Imaging of the Intracellular Assembly of a Functional Viral RNA Replicase Complex

Isabel Fernández de Castro
Centro Nacional de Biotecnología (CNB-CSIC), Spain

José J. Fernández
Centro Nacional de Biotecnología (CNB-CSIC), Spain

Daniel Barajas
University of Kentucky, daniel.barajas@uky.edu

Peter D. Nagy
University of Kentucky, pdnagy2@uky.edu

Cristina Risco
Centro Nacional de Biotecnología (CNB-CSIC), Spain

© 2017. Published by The Company of Biologists Ltd | Journal of Cell Science (2017) 130, 260-268 doi:10.1242/jcs.181586

SPECIAL ISSUE: 3D CELL BIOLOGY

TOOLS AND TECHNIQUES

Three-dimensional imaging of the intracellular assembly of a functional viral RNA replicase complex

Isabel Fernández de Castro[1,‡], José J. Fernández[2], Daniel Barajas[3,*], Peter D. Nagy[3] and Cristina Risco[1,‡]

ABSTRACT

Positive-strand RNA viruses, which can be devastating pathogens in humans, animals and plants, replicate their genomes on intracellular membranes. Here, we describe the three-dimensional ultrastructural organization of a tombusvirus replicase in yeast, a valuable model for exploring virus–host interactions. We visualized the intracellular distribution of a viral replicase protein using metal-tagging transmission electron microscopy, a highly sensitive nanotechnology whose full potential remains to be developed. These three-dimensional images show how viral replicase molecules are organized when they are incorporated into the active domains of the intracellular replication compartment. Our approach provides a means to study protein activation mechanisms in cells and to identify targets for new antiviral compounds.

KEY WORDS: 3D electron microscopy, Tomography, Metal-tagging transmission electron microscopy, Clonable tag, Viral replication factory

INTRODUCTION

The life of the cell depends on compartmentalized interactions of macromolecular assemblies. Shortly after synthesis, proteins must travel from ribosomes to the locations where they will become active. While moving through crowded intracellular environments, protein molecules participate in many interactions before they integrate into the macromolecular complexes in which they have a specific function. Intracellular pathogens move in this same environment; for example, viruses place their newly synthesized molecules and co-factors at specific intracellular locations where they become fully active for viral genome replication and for assembly of new infectious progeny (Risco et al., 2014). With their high mutation rates, RNA viruses produce a myriad of variants in each replication round (Domingo et al., 2012) that will generate novel interactions with cell components; those with the capacity to produce numerous progeny or to hide efficiently from cell defenses will usually prevail.

In the long history of random interactions between viruses and cells, the use of endomembranes for viral genome replication is a distinctive achievement of the RNA viruses. All positive-strand (+)RNA viruses and some negative-strand RNA and double-stranded (ds)RNA viruses replicate their genomes in intracellular membranous platforms (den Boon and Ahlquist, 2010; de Castro et al., 2013). Cell membranes shelter viral genome replication from host antiviral compounds (Wileman, 2006; Miller and Krijnse-Locker, 2008; Romero-Brey et al., 2012; Xu and Nagy, 2014). These co-opted subcellular membranes also concentrate viral and subverted host components, facilitating efficient assembly of viral replicase complexes (VRCs). Until recently, viruses were considered incapable of fabricating membranes; now we know that some viruses produce membranous scaffolds by manipulating cell lipid metabolism and transport (Hsu et al., 2010; Netherton and Wileman, 2011; Reiss et al., 2011; Paul et al., 2014). Viral RNA polymerases are key early factors in the biogenesis of replication factories, where specific cell elements, such as mitochondria, are recruited and work for the virus (Claus et al., 2011; Romero-Brey et al., 2012; de Castro et al., 2013).

To understand the complex biogenesis of viral replication platforms, new imaging approaches are needed. Three-dimensional (3D) microscopy is a powerful tool for the study of viruses in cells (Risco et al., 2014). Detailed characterization of organelle and viral structure biogenesis in cells requires 3D molecular mapping techniques. We developed a labeling method, metal-tagging transmission electron microscopy (METTEM), that uses the metal-binding protein metallothionein as a genetically clonable tag for visualization of proteins in cells with high sensitivity (Fernández de Castro et al., 2014). Mouse metallothionein 1 (used here as the metalliothionein tag), a 61-amino-acid protein, comprises 20 cysteine residues that bind to metal atoms very efficiently. When fused with a protein of interest and treated *in vitro* with gold salts, a single metallothionein tag will build an electron-dense gold-thiolate cluster 1 nm in diameter (Mercogliano and DeRosier, 2006, 2007). We transferred this procedure to live cells and have shown previously that METTEM can be used to label intracellular proteins in bacteria (Diestra et al., 2009), mammalian cells (Risco et al., 2012) and yeast (Barajas et al., 2014a). We have also demonstrated previously that heavy metals are transported into cells with the efficiency necessary to allow gold cluster formation, and that non-specific background from resident endogenous metallothionein is negligible (Fernández de Castro et al., 2014).

This approach allows new possibilities for electron microscopy analysis of macromolecular complexes in cells (Diestra et al., 2009; Delebecque et al., 2011; Risco et al., 2012; Barajas et al., 2014a) and has permitted identification of virus-induced organelles (Risco et al., 2012; Barajas et al., 2014a,b). Here, we used METTEM to study the 3D organization of the replication platform built by a plant virus, the tomato bushy stunt virus (TBSV), in yeast. The yeast model has been helpful in clarifying the role of host factors that facilitate (+)RNA virus replication and infection (Nagy et al., 2014). The yeast *Saccharomyces cerevisiae* can provide all or most of the functions required for successful plant virus replication, establishing a simpler model in which to study the interactions of plant viruses with their hosts (Nagy, 2008).

In the present work, we have chosen the Δpah1 yeast strain because TBSV replicates better in these cells. Pah1 (SwissProt ID

[1]Cell Structure Laboratory, Centro Nacional de Biotecnología (CNB-CSIC), Campus de Cantoblanco, Madrid 28049, Spain. [2]Department of Structure of Macromolecules, Centro Nacional de Biotecnología (CNB-CSIC), Campus de Cantoblanco, Madrid 28049, Spain. [3]Department of Plant Pathology, University of Kentucky, Lexington, Kentucky, KY 40546, USA.
*Present address: BioMarin Pharmaceutical, Novato, CA 94949, USA.

[‡]Authors for correspondence (crisco@cnb.csic.es; ifernandez@cnb.csic.es)

Received 5 November 2015; Accepted 18 March 2016

Journal of Cell Science

Journal of Cell Science (2017) 130, 260-268 doi:10.1242/jcs.181586

P32567) is a phosphatidate phosphatase that regulates cell membrane biogenesis and lipid storage (Csaki and Reue, 2010). Lack of pah1 protein causes proliferation of endoplasmic reticulum (ER) membranes in yeast (Siniossoglou, 2009); in these conditions, the site of TBSV replication switches from peroxisomes to the greatly expanded ER, which is effectively subverted by the virus (Chuang et al., 2014). Using METTEM and 3D imaging, we visualized the viral replicase molecules inside Δpah1 yeast cells and studied their organization as they were incorporated into the active sites of the membrane viral factory.

RESULTS

Efficient assembly of the TBSV VRC in Δpah1 yeast has enabled detailed structural characterization of the viral replication platform. In wild-type yeast, viruses replicate in discrete peripheral membranous structures in which the viral replicase accumulates (Fig. 1A,B). These compartments correspond to peroxisome-derived multivesicular bodies (MVB), the Tombusvirus replication organelles in plant cells and yeast (McCartney et al., 2005; Barajas et al., 2014a). Serial sectioning, transmission electron microscopy (TEM), 3D reconstruction and image processing showed that MVB are interconnected with membranes and surrounded by mitochondria (Fig. 1C). In Δpah1 yeast cells, ultrastructural analysis showed an expanded ER compartment that occupies large areas of the cell (Fig. 1D,E); stacks of ER membranes surround groups of vesicles reminiscent of the peroxisome-derived MVB (Fig. 1D,E). 3D imaging using serial sections and TEM indicated that the viral 'MVBs' that assemble in Δpah1 yeast cells are surrounded by, and remain attached to, stacked ER membranes (Fig. 1F). Immunogold labeling of serial sections showed that

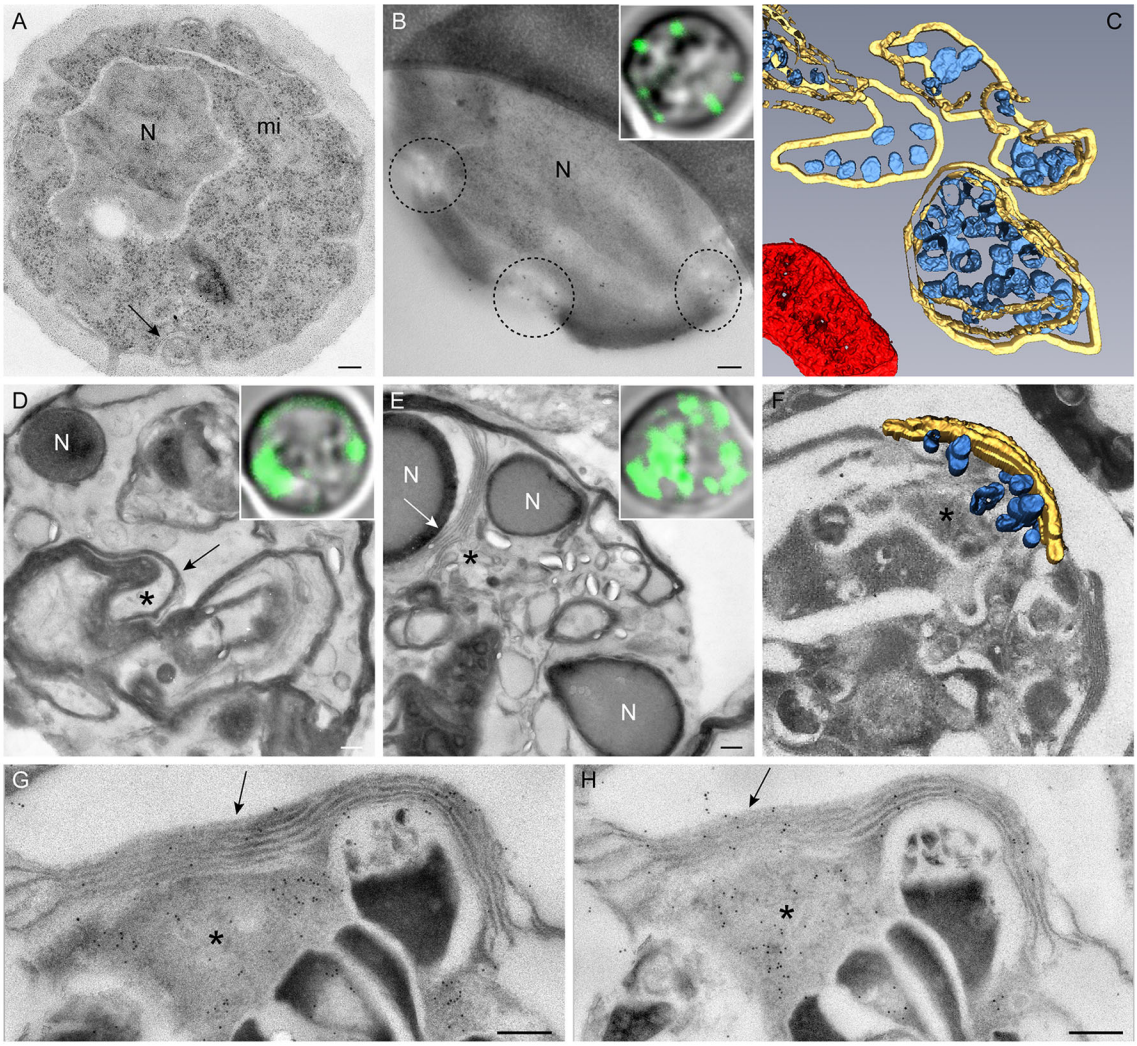

Fig. 1. TEM of the tombusvirus replication platform in yeast. (A–C) Wild-type yeast cells (BY4741) replicating TBSV repRNA. (A) Low-magnification view showing wild-type cell ultrastructure with membranous structures at the cell periphery (arrow). (B) Viral replication complexes (VRC) are peripheral multivesicular bodies (MVB; dashed circles). His-tagged p33 replicase protein was detected with antibodies against His tag in immunogold assays. p33–GFP (green) in a different cell was visualized by confocal laser fluorescence microscopy (inset). (C) TEM of serial sections, 3D reconstruction and image processing show peripheral MVB (yellow) with characteristic spherules (blue); a mitochondrion is shown (red). (D,E) Δpah1 yeast replicating TBSV repRNA, showing fragmented nuclei and expanded membranous compartments (asterisks) surrounded by stacked ER elements (arrows). In Δpah1 yeast, p33-GFP replication protein molecules occupy large regions coincident with the expanded ER (insets). (F) TEM 3D reconstruction and image processing of serial sections show that the large membranous compartment (asterisk) contains MVB-like structures with spherules (blue) surrounded by stacked ER (yellow). (G,H) Serial sections and immunogold labeling with an antibody against dsRNA and a secondary antibody conjugated with 10-nm colloidal gold particles. Signals are intense inside the MVB (asterisks) and weaker in the surrounding ER membranes (arrows). N, nuclei; mi, mitochondria. Scale bars: 200 nm (A,B,D,E); 100 nm (H).

Journal of Cell Science (2017) 130, 260-268 doi:10.1242/jcs.181586

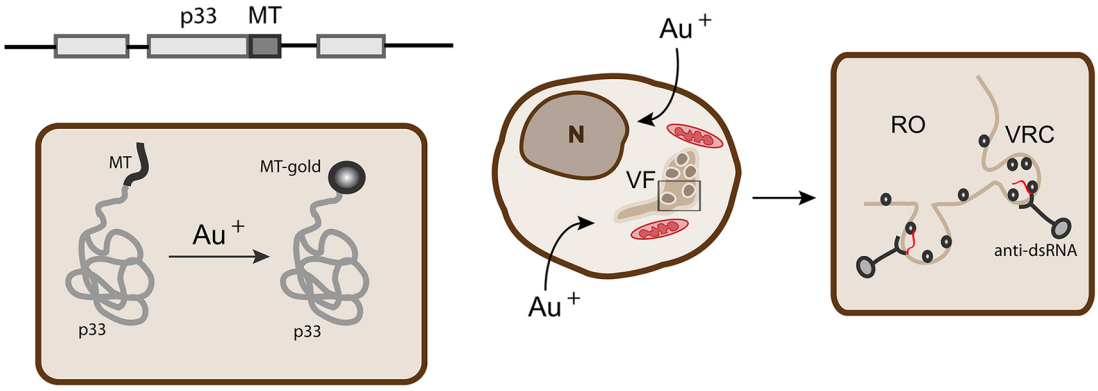

Fig. 2. Imaging VRC molecular biogenesis with METTEM technology. p33 replicase protein fused with metallothionein (MT) is expressed in yeast as a component of an active TBSV replicon. repRNA was expressed separately, as described previously (Barajas et al., 2014a). Cells were incubated with gold salts *in vivo* for construction of gold nanoparticles and processed with TEM analysis of ultrathin sections. Gold nanoparticles show the precise location of p33–metallothionein molecules inside viral factories (VF), replication organelles (RO) and in viral replication complexes (VRC), whose activity is marked with antibodies against dsRNA in immunogold assays.

signals associated with antibodies detecting dsRNA, used as a marker of viral replication, concentrate in the interior of these MVB-like structures (Fig. 1G,H).

For detailed characterization of the viral replication platform, we used METTEM to locate the most abundant VRC component, the TBSV p33 protein (SwissProt ID P15962) (Fig. 2). p33 was fused

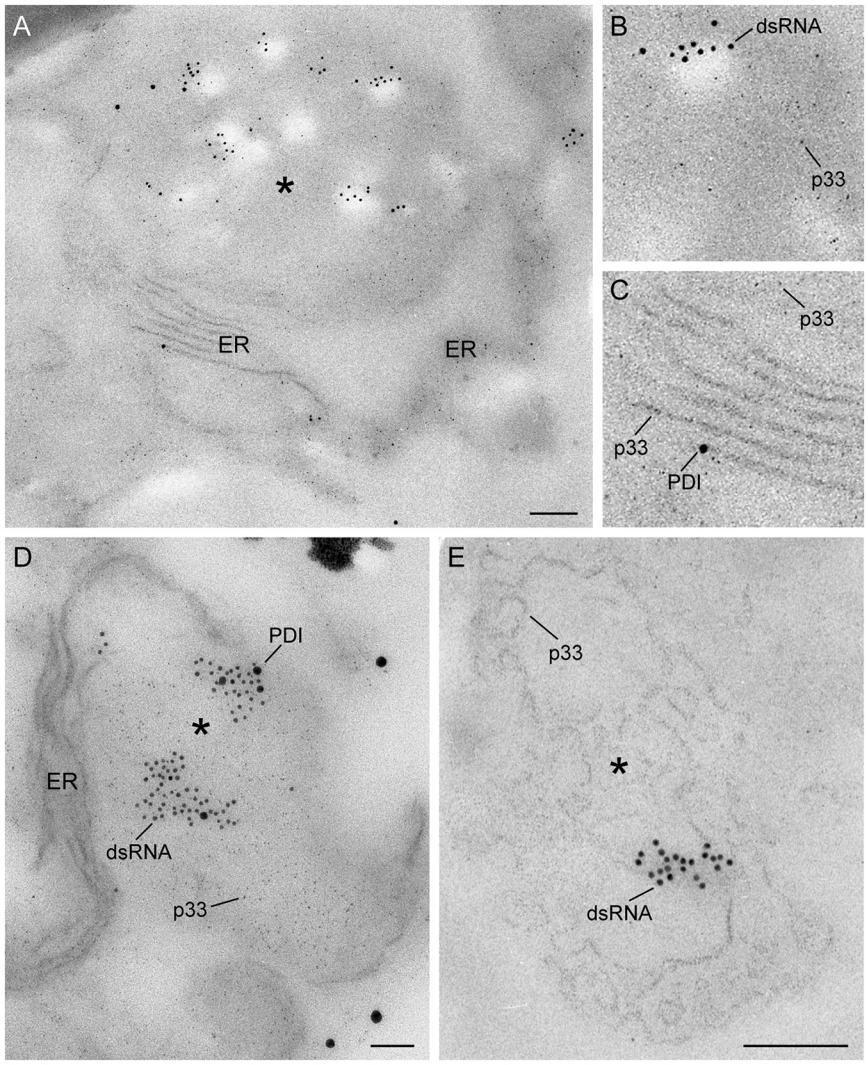

Fig. 3. METTEM-mediated visualization of p33–metallothionein molecules in the TBSV replication platform of Δpah1 yeast. Sections were not stained in order to avoid masking metallothionein nanoclusters. (A) p33–metallothionein–gold nanoparticles (~1 nm) were detected inside MVBs (asterisk) and in the surrounding ER membranes. Replicating TBSV repRNA was labeled with antibodies against dsRNA and a secondary antibody conjugated to 5-nm gold particles. PDI, an ER membrane marker, was visualized with a specific antibody and secondary antibody conjugated to 10-nm gold particles. (B,C) Close-ups of two regions of the image in A. (D,E) Similar replication platforms from different cells. In the absence of staining, membranes of the replication platform were delineated by the abundant p33–metallothionein–gold nanoparticles. Scale bars: 100 nm.

Journal of Cell Science (2017) 130, 260-268 doi:10.1242/jcs.181586

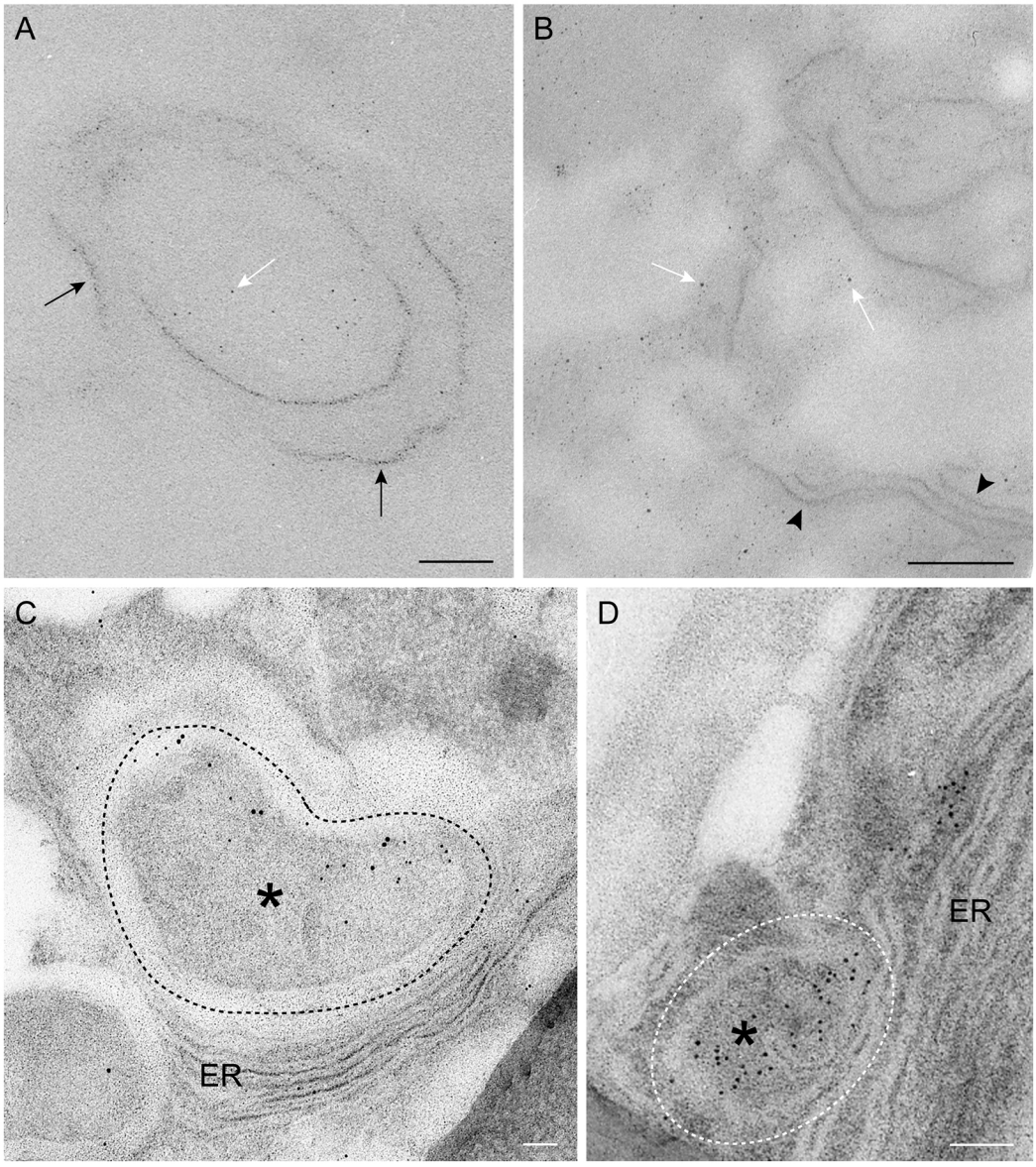

Fig. 4. Distribution of p33-metallothionein molecules in the TBSV replication platform. (A,B) Non-stained sections. Gold nanoparticles that associated with p33–metallothionein molecules (white arrows) outline membranes (black arrows) and stacked ER (black arrowheads). (C,D) Stained sections. Immunogold labeling with antibodies to the ER marker PDI (10-nm colloidal gold particles) and dsRNA (5-nm colloidal gold particles). Labeling signals concentrates in the MVB internal domains (asterisks). Dashed lines delineate the MVB. Scale bars: 100 nm.

with the metallothionein tag and expressed in yeast as a viral replicon component. Transformed yeast cells expressing p33–metallothionein were treated with gold salts to form metallothionein–gold nanoclusters and processed for embedding, ultra-thin sectioning and TEM visualization; sections were also processed for immunogold labeling of viral proteins, cell markers and dsRNA. Electron microscopy imaging showed the precise location of p33–metallothionein molecules in the ER compartment and the MVB (Fig. 3). The electron-dense gold nanoclusters associated with p33–metallothionein molecules were detected in the membranous compartment, as visualized in 2D and 3D TEM images (Figs 1, 3 and 4A,B). Within the replication platform, p33–metallothionein–gold nanoparticles outlined stacked ER membranes and 'MVBs' (Fig. 3A–C). Analysis of >80 cells showed that immunogold signals of antibodies detecting dsRNA concentrated inside the 'MVB' (Figs 3A,D and 4C,D); signals were weaker in surrounding stacked ER membranes, which also contained many p33 molecules (Figs 3A,C and 4C,D). Immunogold labeling with antibodies specific for an ER marker confirmed that the 'MVBs' are closely related to and connected with the surrounding stacked ER membranes (Fig. 3A,D).

For more precise details, we studied the entire platform in three dimensions with electron tomography (Figs 5 and 6). Nine tomograms showed that the replication platform internal domains contained p33–metallothionein molecules in a variety of aggregation states (Figs 5A and 6A,B; Movies 1, 2). Given their location and diameter, these internal domains seen in 3D probably correspond to the 'MVB' areas with spherules, as seen in 2D images (compare Fig. 5A with Fig. 3D, and Fig. 6C with Fig. 3A and Fig. 4C). An initial impression from analysis of these tomograms was that p33 molecules were more densely packed inside MVB-like structures, where the highest replication level was mapped (Fig. 5A; Movie 1).

Journal of Cell Science (2017) 130, 260-268 doi:10.1242/jcs.181586

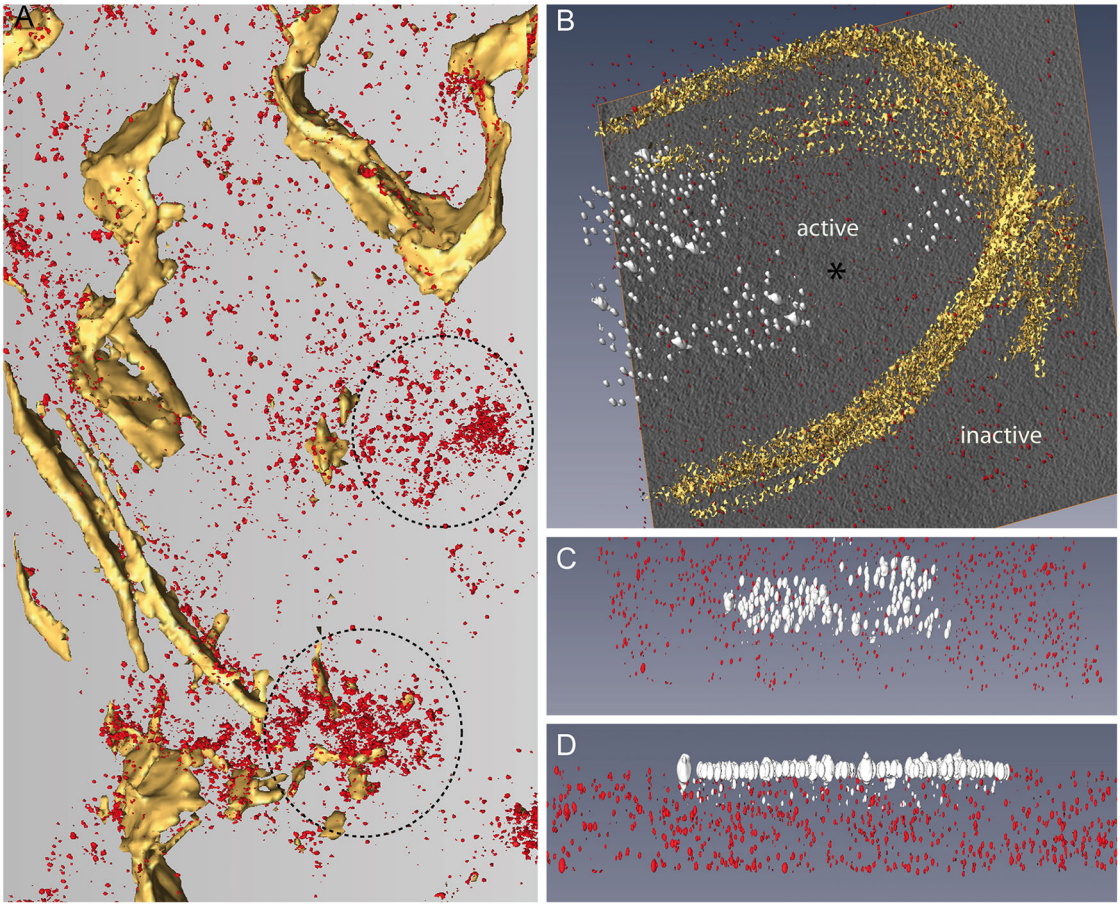

Fig. 5. Molecular organization of the TBSV replication platform in 3D as shown by electron tomography of Δpah1 yeast. (A) TBSV p33–metallothionein–gold molecules (red). Replicase molecules in a variety of aggregation states were seen in the internal domain of the platform (dotted circles) surrounded by ER membranes (yellow). (B) Electron tomography of active VRC within the replication platform. Sections were processed by immunogold labeling with antibodies against dsRNA and colloidal gold conjugates (white), and visualized using electron tomography. p33–metallothionein–gold molecules (red), ER membranes (yellow). The antibodies label the active domain (asterisk) within the replication compartment surrounded by ER membranes. The domain beyond the ER boundaries does not label (inactive). (C,D) Views of the tomogram in B, showing one domain labeled with an antibody against dsRNA. The lateral view in D clearly shows the antibodies bound to their antigens on the section surface, whereas p33 molecules (red) were detected inside the section. See also Movies 1, 2 and 3.

To test this observation directly, samples were processed for immunogold labeling with dsRNA-specific antibodies and visualized with electron tomography. Image processing of the tomograms showed the detailed organization of p33 molecules in active VRCs (Figs 5B–D and 7). The 3D analysis of the nine labeled 'MVBs' showed that p33 molecules did not pack more densely beneath the antibodies recognizing dsRNA than in stacked ER membranes, where labeling was clearly weaker (Fig. 5B–D; Movies 3 and 4).

DISCUSSION

Labeling protein molecules in 3D maps of cells is a major challenge in structural cell biology. We show that the METTEM method, combined with other techniques, can be used to determine the aggregation state of viral polymerase molecules and to establish associations with their activation conformation (Fig. 8). This approach allows the molecular mapping of volumes that had not been achieved to date.

TBSV shows high replication activity in the Δpah1 yeast strain, which lacks the *PAH1* lipin gene, the homolog of the mammalian fat-regulating protein lipin-1 (Carman and Han, 2011). Lipins are phosphatidate phosphatases that have key roles in cell membrane biogenesis (Csaki and Reue, 2010). The high-resolution METTEM technique allowed us to characterize the TBSV replication platform in Δpah1 yeast; we detected the p33 replicase with exceptional sensitivity. In wild-type yeast, viruses replicate in single-membrane vesicles (viral spherules) that are generated from peroxisome membranes. p33 molecules colocalize with replicating TBSV replicon RNA (repRNA) in these vesicles, as detected using antibodies against dsRNA (Barajas et al., 2014a). We found that in Δpah1 yeast, however, MVB and viral spherules are associated with ER membranes, and assemble a replication platform whose dimensions and lipid composition are optimal for TBSV propagation. Our results here strongly suggest that viral replicase molecules become fully active in the MVB internal vesicular domains, where they can adopt appropriate conformations, states of aggregation and/or encounter necessary co-factors.

The increase in viral replication observed in Δpah1 yeast could be due to the presence of a larger surface for replication organelle assembly and to the association between the modified compartment with ER, which allows generation of a highly specialized network. Compartmentalizing the phases of the viral cycle in a specific area of the cell might optimize the process of viral multiplication.

Journal of Cell Science (2017) 130, 260-268 doi:10.1242/jcs.181586

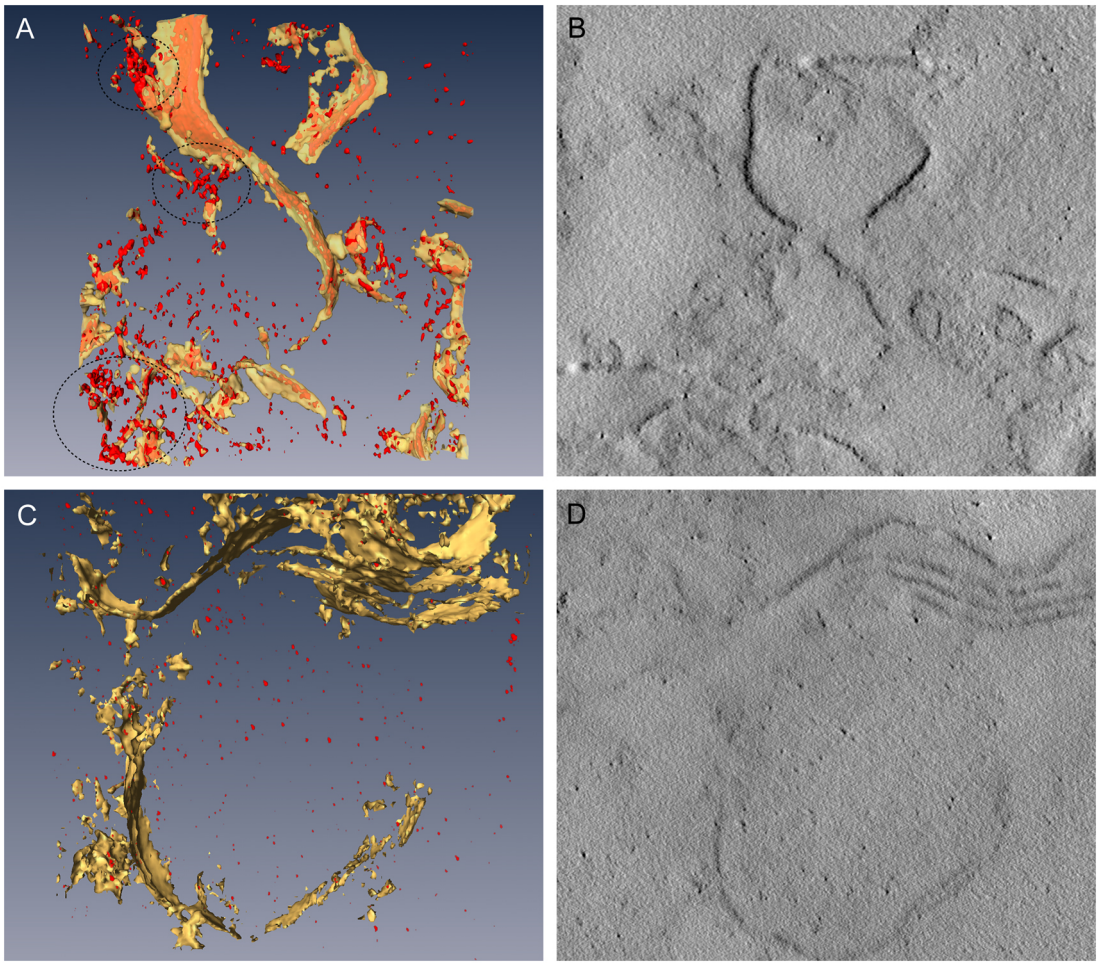

Fig. 6. Analysis of electron tomography volumes of the replication platform. (A,C) 3D models and (B,D) computational tomographic slices corresponding to two replication platforms. Membranes are shown in yellow and p33–metallothionein–gold molecules in red. In A, transparent yellow emphasizes the p33–metallothionein–gold molecules that outline the membranes. Dashed circles show aggregates of p33–metallothionein–gold molecules.

The described membranous network is reminiscent of other structures generated by flaviviruses, coronaviruses and arteriviruses, which assemble different types of vesicles from the ER to generate a platform comprising interconnected structures (Risco et al., 2014). This modified ER can harbor viral replication, store newly synthesized viral genome or support assembly of new viruses. In addition, it could facilitate transport of components between different MVB regions. To replicate, the virus thus requires certain membrane compositions, of which lipids are a key component; virus-mediated changes directly affect the main features of intracellular membranes.

The 3D model showed different amounts of viral replicase molecule aggregation, depending on the location in the compartment. The approaches used here allowed us to show that p33 activity does not depend on its state of packing. Our data indicate that the compartment is divided into domains in which the protein is active, regardless of molecule aggregation. Previous studies have suggested that close packing or oligomeric association of RNA-dependent RNA polymerase molecules is important for viral RNA replication in cells (Lyle et al., 2002; Spagnolo et al., 2010; Risco et al., 2012). This fundamental step in viral multiplication nonetheless depends on the specific virus and cell host. Here, we show that, when being incorporated into the active domains of the replication platform, TBSV replicase molecules do not markedly change their aggregation state. Interaction with specific co-factors must thus be the most crucial step for VRC activation in specific replication organelle domains (summarized in Fig. 8). Because new peroxisomes are born in the ER (Tabak et al., 2013), our results suggest that the structures harboring the TBSV active VRC are nascent peroxisomes whose detachment from the ER is blocked. This generates a secluded compartment where replicated viral RNA is protected and where replicases meet their co-opted co-factors, lipids and suitable membranous microdomains.

The impact of RNA viruses can be limited by preventing their replication. The study of how intracellular pathogens manipulate lipid traffic and membrane biogenesis is an expanding research area (Sarowar et al., 2009; Mutsafi et al., 2013; Barajas et al., 2014b; Konan and Sanchez-Felipe, 2014; Nour and Modis, 2014; Paul et al., 2014). We show the importance of 3D imaging when combined with new methods for sensitive molecular mapping to better understand viral replication in cells. Our technologies will allow fundamental questions to be addressed regarding membrane dynamics and how viruses subvert underlying lipid-trafficking machineries. These studies will assist in the structure-guided design of molecules that interfere with the macromolecular organization of

Journal of Cell Science (2017) 130, 260-268 doi:10.1242/jcs.181586

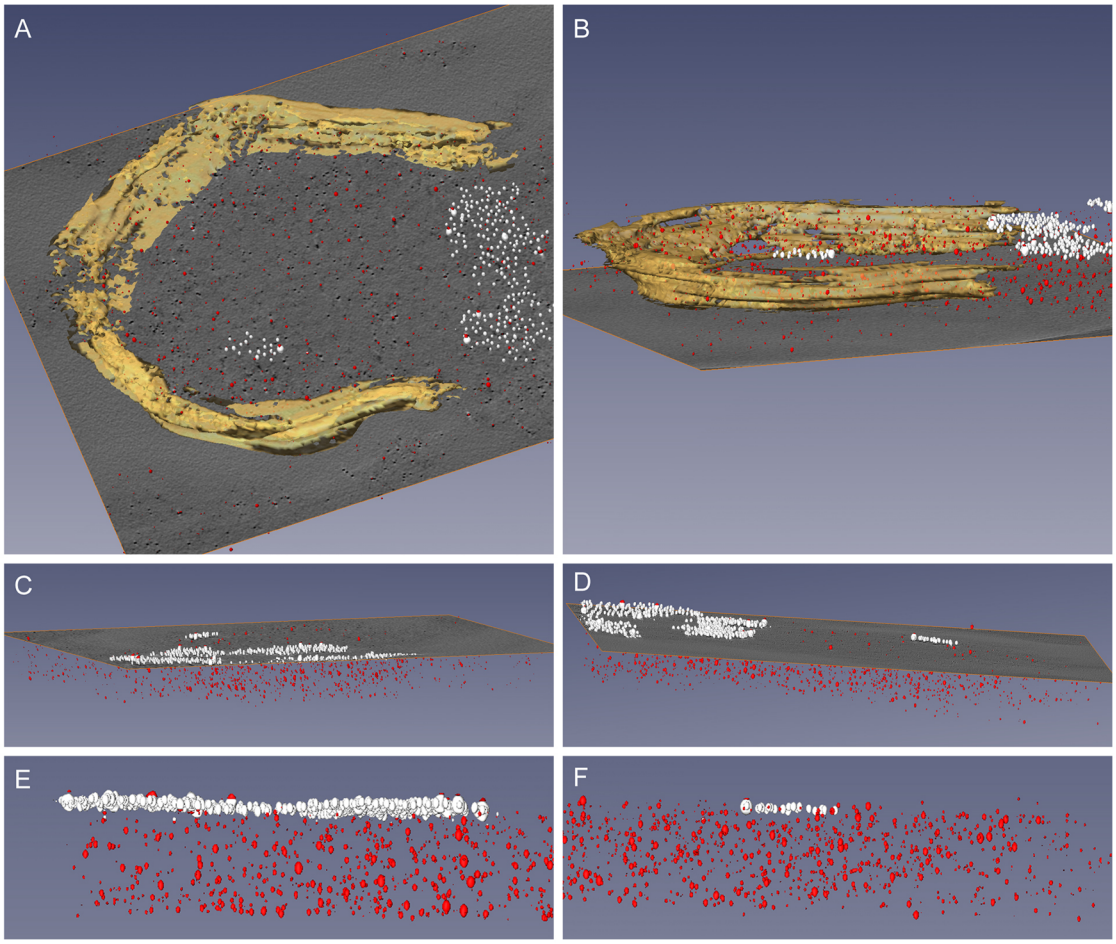

Fig. 7. Electron tomography of a replication platform that had been stained with antibodies against dsRNA and gold-conjugated secondary antibodies. (A,B) Different views of a 3D model showing the distribution of ER membranes (yellow), p33–metallothionein–gold molecules (red) and dsRNA-specific antibodies labeled with colloidal-gold-conjugated secondary antibodies (white). (C–F) Lateral views of the volume showing the antibodies bound to the section surface and p33 molecules inside the section. See also Movie 4.

replicases and their co-factors in live cells, leading to the emergence of a new generation of anti-viral compounds. In addition, these methods will help to resolve an open question in cell biology (Travis, 2011): how cells localize their proteins and how these become fully active in the natural environment of the living cell.

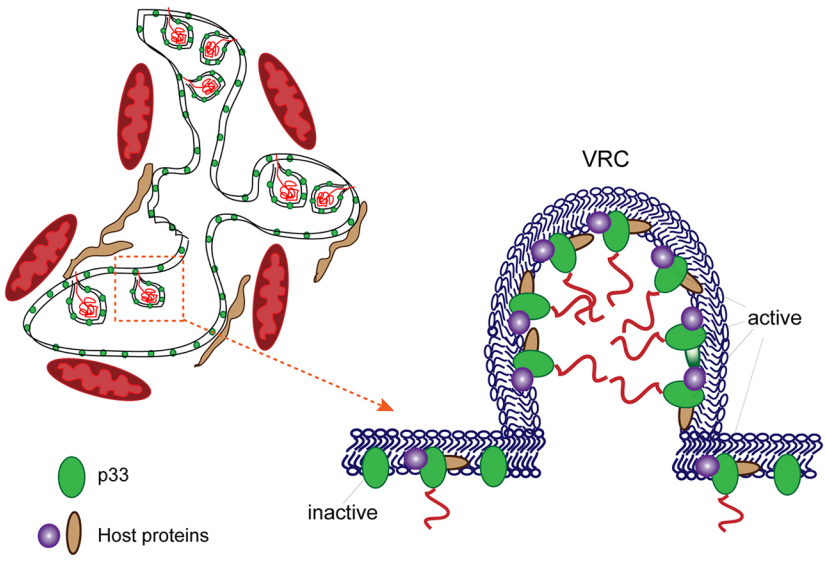

Fig. 8. Organization of TBSV replication organelles. The TBSV replication platform in Δpah1 yeast is built of MVB attached to stacked ER membranes. MVB might be nascent peroxisomes whose detachment from ER is blocked. The ER-membrane-surrounded secluded compartment contains the VRCs that protect the replicated viral RNA. Replicase molecules incorporate into both ER and MVB membranes. RNA replication occurs in sites where viral replicases meet their co-opted co-factors, lipids and suitable membrane microdomains.

Journal of Cell Science (2017) 130, 260-268 doi:10.1242/jcs.181586

MATERIALS AND METHODS

Yeast strains, cell culture and sample preparation

Saccharomyces cerevisiae strain RS453 (*MATa ade2-1 his3, 15 leu2-3, 112 trp1-1 ura3 52*) and pah1Δnem1Δ (SwissProt ID for Nem1 is P38757) (pah1Δ::TRP1nem1Δ::HIS3 derivative of RS453) have been reported previously (Choi et al., 2011; Barajas et al., 2014b). For expression of TBSV replicases and assembly of the functional replication complex, wild-type RS453 and pah1Δnem1Δ yeast strains were transformed with pESC-HIS-metallothionein-p33/FLAGp92 (*LEU* selection) and pYC-DI72 (*URA* selection). Yeast were pre-grown in 2 ml of yeast extract peptone galactose (YPG) and shaken overnight (250 rpm, 30°C). To induce and maintain viral replication, yeasts cells were cultured for 24 h in YPG (250 rpm, 23°C). When OD_{600} was ∼2, cells were harvested in Tris-sulfate with dithiothreitol (DTT) (TSD) reduction buffer, pH 9.4, to facilitate cell wall digestion. To obtain spheroplasts, yeast were incubated (10 min, 30°C) with 0.1 mg/ml zymolyase 20 T (AMS Biotechnology), followed by three washes with spheroplast medium A [1× yeast nitrogen base, 2% (w/v) glucose, 1× amino acids, 1 M sorbitol, 20 mM Tris-HCl, pH 7.5].

Electron microscopy

For ultrastructural studies, spheroplasts were fixed (20 min) in a mixture of 8% paraformaldehyde and 1% glutaraldehyde in HEPES (pH 7.4), followed by a second fixing step (1 h) with 4% paraformaldehyde and 0.5% glutaraldehyde in the same buffer. Cells were post-fixed (1 h, 4°C) with 1% osmium tetroxide and 0.8% potassium ferricyanide in water. After several washes with HEPES, samples were incubated (40 min, 4°C) with 2% uranyl acetate. Cells were dehydrated in 20-min steps, with increasing concentrations of acetone (50, 70, 90 and twice in 100%) at 4°C, then incubated with a 1:1 mixture of acetone-resin (epoxy resin EML-812; Taab Laboratories) with gentle agitation at room temperature. Cells were infiltrated overnight in pure resin and polymerized (48 h, 60°C). Ultrathin (50–70 nm) sections were collected on 300-mesh copper grids (G300-C3, Taab) and stained with saturated uranyl acetate and lead citrate.

To visualize metallothionein-tagged p33 in cells, we incubated spheroplasts (75 min) with 2 mM $HAuCl_4$ (Sigma-Aldrich) in spheroplast medium A. This treatment builds gold nanoclusters in metallothionein-tagged proteins, allowing highly sensitive detection of protein molecules in cells (Risco et al., 2012; Fernández de Castro et al., 2014). Cells were washed with spheroplast medium A before fixing (1 h, room temperature) with 4% paraformaldehyde and 0.2% glutaraldehyde in PHEM solution (20 mM PIPES, 50 mM HEPES, 20 mM EGTA and 4 mM $MgCl_2$, pH 6.9). Cells were dehydrated in short steps (10 min each) in increasing ethanol concentrations (30, 50, 70, 90 and twice in 100%) at 4°C, then embedded in LR-White acrylic resin. Spheroplasts were incubated in mixtures of ethanol–LR-White (2:1, 1:1, 1:2) with gentle agitation and protected from light, then embedded in 100% resin (24 h). Samples were polymerized (48 h, 60°C), and ultrathin sections were collected on 300-mesh Quantifoil holey carbon grids (R 3.5/1 Cu/Rh, Quantifoil Micro Tools) and studied without staining. Labeling specificity was confirmed as described previously (Risco et al., 2012; Barajas et al., 2014a; Fernández de Castro et al., 2014).

For immunogold labeling, LR-White-embedded cell sections were processed as described previously (Risco et al., 2002; Barajas et al., 2014a). Briefly, sections were incubated (6 min) with 1% bovine serum albumin (BSA) in PBS, with primary antibodies diluted in 1% BSA and secondary antibodies conjugated with colloidal gold particles (5 or 10 nm; BB International) diluted in 1% BSA. Antibodies used were rabbit anti-PDI M-12 (1:200; Sigma-Aldrich), mouse anti-dsRNA monoclonal antibody J2 (1:200; English & Scientific Consulting) and mouse anti-polyhistidine H1029 (1:100; Sigma-Aldrich). Secondary antibodies were diluted 1:40. Samples were studied with a Jeol JEM 1011 electron microscope operating at 100 kV.

Serial sectioning and 3D reconstruction

Consecutive ultrathin (60–70 nm) sections were collected on Formvar-coated copper slot grids (Taab Laboratories), stained and imaged with TEM. Series were processed for 3D reconstruction as described previously (Fontana et al., 2008). Photographs were taken at 10,000 or 12,000 nominal magnification. Plates were digitized as 8-bit images with a 3.39-nm final pixel size and 600 dpi resolution with an Epson Perfection Photo 3170 scanner. Digital images were aligned using selected tracers between two consecutive sections with the free editor for serial section microscopy Reconstruct (Fiala, 2005) (http://synapses.clm.utexas.edu/tools/index.stm). Noise was reduced with three rounds of median filter, segmentation and 3D visualization using Amira software (http://amira.zib.de). Resolution in the *Z*-axis, in this case ∼50 nm, was limited by section thickness and by alignment quality.

Electron tomography and image processing

Thick sections (∼300 nm) were taken on Quantifoil R3.5/1 Cu/Rh grids. Tilt series were collected automatically at 1.5° increments over an angular range of −63° to +60° on FEI Tecnai G2 F20 and Tecnai Spirit Twin microscopes (FEI, Eindhoven, The Netherlands). Accelerating voltage was 200 and 120 kV, respectively.

Tilt series alignment and tomographic reconstruction was performed with IMOD software (Kremer et al., 1996). For final segmentation and 3D visualization, Amira software was used. Noise reduction and automated segmentation programs helped to highlight membrane visualization (Martinez-Sanchez et al., 2011, 2013, 2014).

Acknowledgements

We thank Drs Martin Sachse, Nihal Altan-Bonnet and Andrew White for valuable discussions and expert revision of the manuscript; Carmen López-Iglesias for support with electron tomography analysis; Judit Pogany and Chingkai Chuang for technical support; and Catherine Mark for editorial assistance.

Competing interests

The authors declare no competing or financial interests.

Author contributions

I.F.d.C. designed and conducted experiments, analyzed and interpreted data, made the figures. C.R. designed and supervised experiments, interpreted data and wrote the manuscript. J.J.F. supervised 3D reconstructions and image processing work, and analyzed data. D.B. and P.D.N. provided yeast strains and plasmids, and read the manuscript. All authors commented on and approved the manuscript.

Funding

This work was supported by the Spanish Ministry of Economy and Competitiveness [grant numbers BIO2012-33314 to C.R. and TIN2012-37483 to J.J.F.]; and the US National Science Foundation [grant number MCB-1122039 to P.D.N.].

Data availability

Supplementary material movies are available at https://dx.doi.org/10.6084/m9.figshare.3159094.v1

Supplementary information

Supplementary information available online at
http://jcs.biologists.org/lookup/doi/10.1242/jcs.181586.supplemental

References

Barajas, D., Martín, I. F. d. C., Pogany, J., Risco, C. and Nagy, P. D. (2014a). Noncanonical role for the host Vps4 AAA+ ATPase ESCRT protein in the formation of tomato bushy stunt virus replicase. *PLoS Pathog.* **10**, e1004087.

Barajas, D., Xu, K., de Castro Martín, I. F., Sasvari, Z., Brandizzi, F., Risco, C. and Nagy, P. D. (2014b). Co-opted oxysterol-binding ORP and VAP proteins channel sterols to RNA virus replication sites via membrane contact sites. *PLoS Pathog.* **10**, e1004388.

Carman, G. M. and Han, G.-S. (2011). Regulation of phospholipid synthesis in the yeast Saccharomyces cerevisiae. *Annu. Rev. Biochem.* **80**, 859-883.

Choi, H.-S., Su, W.-M., Morgan, J. M., Han, G.-S., Xu, Z., Karanasios, E., Siniossoglou, S. and Carman, G. M. (2011). Phosphorylation of phosphatidate phosphatase regulates its membrane association and physiological functions in Saccharomyces cerevisiae: identification of SER(602), THR(723), AND SER (744) as the sites phosphorylated by CDC28 (CDK1)-encoded cyclin-dependent kinase. *J. Biol. Chem.* **286**, 1486-1498.

Chuang, C., Barajas, D., Qin, J. and Nagy, P. D. (2014). Inactivation of the host lipin gene accelerates RNA virus replication through viral exploitation of the expanded endoplasmic reticulum membrane. *PLoS Pathog.* **10**, e1003944.

Claus, C., Chey, S., Heinrich, S., Reins, M., Richardt, B., Pinkert, S., Fechner, H., Gaunitz, F., Schafer, I., Seibel, P. et al. (2011). Involvement of p32 and microtubules in alteration of mitochondrial functions by rubella virus. *J. Virol.* **85**, 3881-3892.

Csaki, L. S. and Reue, K. (2010). Lipins: multifunctional lipid metabolism proteins. *Annu. Rev. Nutr.* **30**, 257-272.
de Castro, I. F., Volonté, L. and Risco, C. (2013). Virus factories: biogenesis and structural design. *Cell. Microbiol.* **15**, 24-34.
Delebecque, C. J., Lindner, A. B., Silver, P. A. and Aldaye, F. A. (2011). Organization of intracellular reactions with rationally designed RNA assemblies. *Science* **333**, 470-474.
den Boon, J. A. and Ahlquist, P. (2010). Organelle-like membrane compartmentalization of positive-strand RNA virus replication factories. *Annu. Rev. Microbiol.* **64**, 241-256.
Diestra, E., Fontana, J., Guichard, P., Marco, S. and Risco, C. (2009). Visualization of proteins in intact cells with a clonable tag for electron microscopy. *J. Struct. Biol.* **165**, 157-168.
Domingo, E., Sheldon, J. and Perales, C. (2012). Viral quasispecies evolution. *Microbiol. Mol. Biol. Rev.* **76**, 159-216.
Fernández de Castro, I., Sanz-Sánchez, L. and Risco, C. (2014). Metallothioneins for correlative light and electron microscopy. *Methods Cell Biol.* **124**, 55-70.
Fiala, J. C. (2005). Reconstruct: a free editor for serial section microscopy. *J. Microsc.* **218**, 52-61.
Fontana, J., López-Montero, N., Elliott, R. M., Fernández, J. J. and Risco, C. (2008). The unique architecture of Bunyamwera virus factories around the Golgi complex. *Cell. Microbiol.* **10**, 2012-2028.
Hsu, N.-Y., Ilnytska, O., Belov, G., Santiana, M., Chen, Y.-H., Takvorian, P. M., Pau, C., van der Schaar, H., Kaushik-Basu, N., Balla, T. et al. (2010). Viral reorganization of the secretory pathway generates distinct organelles for RNA replication. *Cell* **141**, 799-811.
Konan, K. V. and Sanchez-Felipe, L. (2014). Lipids and RNA virus replication. *Curr. Opin. Virol.* **9**, 45-52.
Kremer, J. R., Mastronarde, D. N. and McIntosh, J. R. (1996). Computer visualization of three-dimensional image data using IMOD. *J. Struct. Biol.* **116**, 71-76.
Lyle, J. M., Bullitt, E., Bienz, K. and Kirkegaard, K. (2002). Visualization and functional analysis of RNA-dependent RNA polymerase lattices. *Science* **296**, 2218-2222.
Martinez-Sanchez, A., Garcia, I. and Fernandez, J.-J. (2011). A differential structure approach to membrane segmentation in electron tomography. *J. Struct. Biol.* **175**, 372-383.
Martinez-Sanchez, A., Garcia, I. and Fernandez, J.-J. (2013). A ridge-based framework for segmentation of 3D electron microscopy datasets. *J. Struct. Biol.* **181**, 61-70.
Martinez-Sanchez, A., Garcia, I., Asano, S., Lucic, V. and Fernandez, J.-J. (2014). Robust membrane detection based on tensor voting for electron tomography. *J. Struct. Biol.* **186**, 49-61.
McCartney, A. W., Greenwood, J. S., Fabian, M. R., White, K. A. and Mullen, R. T. (2005). Localization of the tomato bushy stunt virus replication protein p33 reveals a peroxisome-to-endoplasmic reticulum sorting pathway. *Plant Cell* **17**, 3513-3531.
Mercogliano, C. P. and DeRosier, D. J. (2006). Gold nanocluster formation using metallothionein: mass spectrometry and electron microscopy. *J. Mol. Biol.* **355**, 211-223.
Mercogliano, C. P. and DeRosier, D. J. (2007). Concatenated metallothionein as a clonable gold label for electron microscopy. *J. Struct. Biol.* **160**, 70-82.
Miller, S. and Krijnse-Locker, J. (2008). Modification of intracellular membrane structures for virus replication. *Nat. Rev.* **6**, 363-374.
Mutsafi, Y., Shimoni, E., Shimon, A. and Minsky, A. (2013). Membrane assembly during the infection cycle of the giant Mimivirus. *PLoS Pathog.* **9**, e1003367.
Nagy, P. D. (2008). Yeast as a model host to explore plant virus-host interactions. *Annu. Rev. Phytopathol.* **46**, 217-242.
Nagy, P. D., Pogany, J. and Lin, J.-Y. (2014). How yeast can be used as a genetic platform to explore virus–host interactions: from 'omics' to functional studies. *Trends Microbiol.* **22**, 309-316.
Netherton, C. L. and Wileman, T. (2011). Virus factories, double membrane vesicles and viroplasm generated in animal cells. *Curr. Opin. Virol.* **1**, 381-387.
Nour, A. M. and Modis, Y. (2014). Endosomal vesicles as vehicles for viral genomes. *Trends Cell Biol.* **24**, 449-454.
Paul, D., Madan, V. and Bartenschlager, R. (2014). Hepatitis C virus RNA replication and assembly: living on the fat of the land. *Cell Host Microbe* **16**, 569-579.
Reiss, S., Rebhan, I., Backes, P., Romero-Brey, I., Erfle, H., Matula, P., Kaderali, L., Poenisch, M., Blankenburg, H., Hiet, M.-S. et al. (2011). Recruitment and activation of a lipid kinase by hepatitis C virus NS5A is essential for integrity of the membranous replication compartment. *Cell Host Microbe* **9**, 32-45.
Risco, C., Rodriguez, J. R., Lopez-Iglesias, C., Carrascosa, J. L., Esteban, M. and Rodriguez, D. (2002). Endoplasmic reticulum-Golgi intermediate compartment membranes and vimentin filaments participate in vaccinia virus assembly. *J. Virol.* **76**, 1839-1855.
Risco, C., Sanmartín-Conesa, E., Tzeng, W.-P., Frey, T. K., Seybold, V. and de Groot, R. J. (2012). Specific, sensitive, high-resolution detection of protein molecules in eukaryotic cells using metal-tagging transmission electron microscopy. *Structure* **20**, 759-766.
Risco, C., Fernández de Castro, I., Sanz-Sánchez, L., Narayan, K., Grandinetti, G. and Subramaniam, S. (2014). 3D imaging of viral infections. *Annu. Rev. Virol.* **1**, 453-473.
Romero-Brey, I., Merz, A., Chiramel, A., Lee, J.-Y., Chlanda, P., Haselman, U., Santarella-Mellwig, R., Habermann, A., Hoppe, S., Kallis, S. et al. (2012). Three-dimensional architecture and biogenesis of membrane structures associated with hepatitis C virus replication. *PLoS Pathog.* **8**, e1003056.
Sarowar, S., Kim, Y. J., Kim, K. D., Hwang, B. K., Ok, S. H. and Shin, J. S. (2009). Overexpression of lipid transfer protein (LTP) genes enhances resistance to plant pathogens and LTP functions in long-distance systemic signaling in tobacco. *Plant Cell Rep.* **28**, 419-427.
Siniossoglou, S. (2009). Lipins, lipids and nuclear envelope structure. *Traffic* **10**, 1181-1187.
Spagnolo, J. F., Rossignol, E., Bullitt, E. and Kirkegaard, K. (2010). Enzymatic and nonenzymatic functions of viral RNA-dependent RNA polymerases within oligomeric arrays. *RNA* **16**, 382-393.
Tabak, H. F., Braakman, I. and van der Zand, A. (2013). Peroxisome formation and maintenance are dependent on the endoplasmic reticulum. *Annu. Rev. Biochem.* **82**, 723-744.
Travis, J. (2011). Mysteries of the cell. How does the cell position its proteins? *Science* **334**, 1048-1049.
Wileman, T. (2006). Aggresomes and autophagy generate sites for virus replication. *Science* **312**, 875-878.
Xu, K. and Nagy, P. D. (2014). Expanding use of multi-origin subcellular membranes by positive-strand RNA viruses during replication. *Curr. Opin. Virol.* **9**, 119-126.

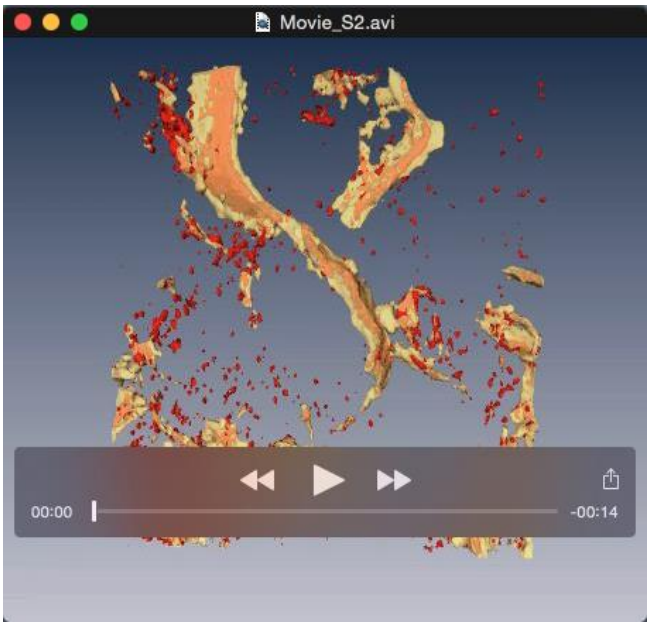

Movies S1-S2. 3D models of the TBSV replication platform as visualized by METTEM and ET (from tomograms in Fig. 5A and Fig. 6A).

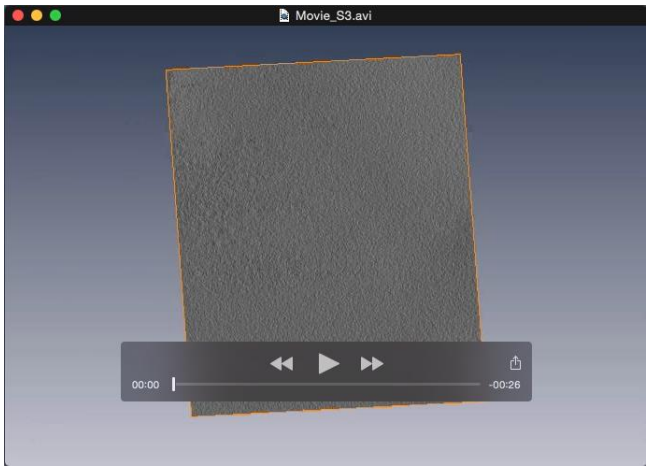

Movie S3. 3D model of a TBSV replication platform as visualized by METTEM immunogold labeling with anti-dsRNA antibodies and ET (from volume in Fig. 5B). The computational slices of the tomogram are first swept upwards (first third of the movie) then backwards (second third), revealing the 3D isosurface representation. The last third of the movie rotates the 3D representation.

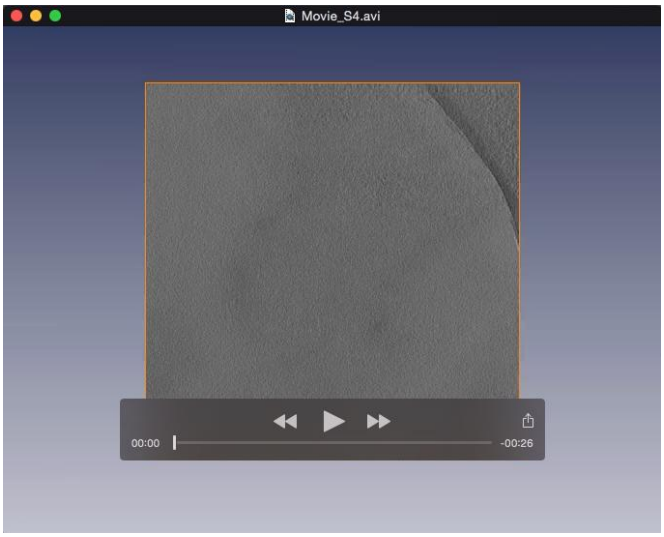

Movie S4. 3D model of a TBSV replication platform as visualized by METTEM immunogold labeling with anti-dsRNA antibodies and ET (from volume in Fig. 7). The computational slices of the tomogram are first swept upwards (first third of the movie) then backwards (second third), revealing the 3D isosurface representation. The last third of the movie rotates the 3D representation.